PHYSICAL REVIEW B **109**, L241105 (2024)

Letter

Topological spin Hall effect in antiferromagnets driven by vector Néel chirality

Kazuki Nakazawa,[1,2] Koujiro Hoshi,[1] Jotaro J. Nakane,[3] Jun-ichiro Ohe,[4] and Hiroshi Kohno[3]

[1]*Department of Applied Physics, The University of Tokyo, Bunkyo, Tokyo 113-8656, Japan*
[2]*RIKEN Center for Emergent Matter Science, Wako, Saitama 351-0198, Japan*
[3]*Department of Physics, Nagoya University, Nagoya 464-8602, Japan*
[4]*Department of Physics, Toho University, 2-2-1 Miyama, Funabashi, Chiba 274-8510, Japan*

(Received 23 March 2023; revised 14 May 2024; accepted 14 May 2024; published 6 June 2024)

Spin Hall effect of spin-texture origin is explored theoretically for antiferromagnetic (AF) metals. Based on the observation that a scalar spin chirality formed by the Néel vector is not a physically well-defined quantity, it is found that a vector chirality formed by the Néel vector gives rise to a topological spin Hall effect. This is topological since it is proportional to the winding number counted by in-plane vector chirality along the sample edge, which corresponds to a homotopy class $\pi_1(S^1)$, instead of $\pi_2(S^2)$ of scalar chirality, and can be nonvanishing for AF merons but not for AF skyrmions. The effect is enhanced when the Fermi level lies near the AF gap, and, surprisingly, at weak coupling with a small AF gap. These features are confirmed numerically based on the Landauer-Büttiker formula. Important roles played by nonadiabatic processes and spin dephasing are pointed out.

DOI: 10.1103/PhysRevB.109.L241105

Spin-charge interconversion has been extensively studied in spintronics with the aim of application to next-generation devices. It is typically achieved by the spin Hall effect (SHE) [1] originating from the relativistic spin-orbit coupling (SOC), mostly in nonmagnetic materials [2–6]. Ferromagnets (FM) are another class of materials that enable spin-charge conversion, not just as a simple spin source but also by emergent electromagnetism due to spatiotemporal magnetization dynamics. In particular, a magnetization texture forming a finite scalar spin chirality simulates a magnetic field that affects electrons' orbital motion [7–11], but in a spin-dependent way. The resulting Hall effect, often called the topological Hall effect (THE), is thus the SHE in essence [12].

Antiferromagnets (AF) are a material having both aspects, magnetic at the microscopic scale but nonmagnetic at the (semi)macroscopic scale, and offers a unique platform to generate pure spin currents. A large SHE was reported in $\mathrm{Ir}_{20}\mathrm{Mn}_{80}$ [14], which originates from SOC. Recently, there are some proposals of SHE that arise from the AF spin texture, providing another means of pure spin-current generation without relying on SOC [15–17].

In this Letter, we explore theoretically the SHE in AF originating from AF spin textures. From an analogy with FM, an AF with a textured Néel vector $\boldsymbol{n}$ is expected to generate a spin Hall current,

$$\tilde{j}^z_{\mathrm{s},i} = \tilde{\sigma}_{\mathrm{SH}}\, \boldsymbol{n}\cdot(\partial_i \boldsymbol{n}\times\partial_j \boldsymbol{n}) e E_j, \tag{1}$$

under an applied electric field E_j. ($\tilde{\sigma}_{\mathrm{SH}}$ is a coefficient, $e>0$ is the elementary charge, and z on $\tilde{j}^z_{\mathrm{s},i}$ indicates the spin component along $\boldsymbol{n}$; see below.) Because of the scalar chirality, $\boldsymbol{n}\cdot(\partial_i \boldsymbol{n}\times\partial_j \boldsymbol{n})$, this effect may be termed a topological spin Hall (TSH) effect. However, $\tilde{j}^z_{\mathrm{s},i}$ changes sign under $\boldsymbol{n}\to-\boldsymbol{n}$, hence it does not express a macroscopically observable quantity. Note that AF states with $\boldsymbol{n}$ and $-\boldsymbol{n}$ are indistinguishable at a macroscopic level. We thus define the physical spin current $\boldsymbol{j}_{\mathrm{s},i}$ through $\tilde{j}^z_{\mathrm{s},i} = \boldsymbol{n}\cdot\boldsymbol{j}_{\mathrm{s},i}$, hence, by

$$j^\alpha_{\mathrm{s},i} = \tilde{\sigma}_{\mathrm{SH}} (\partial_i \boldsymbol{n}\times\partial_j \boldsymbol{n})^\alpha e E_j. \tag{2}$$

The factor $(\partial_i \boldsymbol{n}\times\partial_j \boldsymbol{n})^\alpha$ may be identified as an emergent magnetic field in spin channel, and interestingly, it can be expressed as $(\partial_i a^\alpha_j - \partial_j a^\alpha_i)/2$ with an emergent vector potential,

$$a^\alpha_i = (\boldsymbol{n}\times\partial_i \boldsymbol{n})^\alpha. \tag{3}$$

This is the vector chirality ($\sim \boldsymbol{S}_1\times\boldsymbol{S}_2$ for two spins) formed by the Néel vector, and we call it "vector Néel chirality" [18]. Spatially averaged spin current $\langle j^\alpha_{\mathrm{s},i}\rangle$ is proportional to a winding number defined by the vector chirality, and hence is "topological." To date, the vector spin chirality is known to induce charge [19,20] and (equilibrium) spin currents [21–23], but its AF counterpart in terms of the Néel vector has been less focused on.

In the following, we derive Eqs. (1) and (2) and demonstrate the topological character of the latter. The effect is present in systems with AF merons [24–26] but not with AF skyrmions [27–33], and is enhanced in the weak-coupling regime. These results are confirmed numerically based on the Landauer-Büttiker formula.

We consider electrons hopping on a square lattice and coupled to a given, static spin texture. The Hamiltonian

$$H = -t\sum_{(i,j)} c_i^\dagger c_j - J_{\mathrm{sd}}\sum_i \boldsymbol{S}_i\cdot(c_i^\dagger \boldsymbol{\sigma} c_i) + u_{\mathrm{i}}{\sum_i}' c_i^\dagger c_i \tag{4}$$

consists of nearest-neighbor hopping (first term), *s*-*d* exchange coupling to localized spins $\boldsymbol{S}_i$ (second term), and on-site impurity potential (third term), with electron operators $c_i = {}^t(c_{i\uparrow}, c_{i\downarrow})$ at site i and Pauli matrices $\boldsymbol{\sigma} = (\sigma^x, \sigma^y, \sigma^z)$. We assume an arbitrary slowly varying checkerboard type AF texture, $\boldsymbol{S}_i = S(-1)^i \boldsymbol{n}_i$, where $\boldsymbol{n}_i$ is the Néel vector varying slowly in space [Fig. 1(a)].

2469-9950/2024/109(24)/L241105(6)

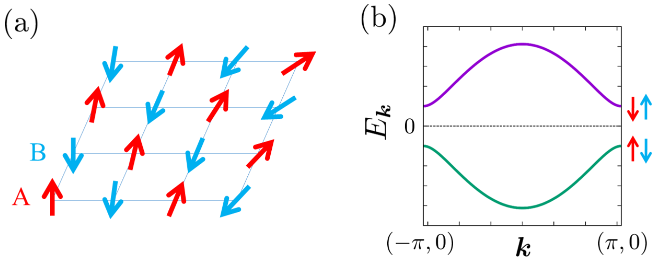

FIG. 1. (a) Static magnetic structure considered in this work, a checkerboard type AF on a square lattice with a very slow spatial modulation. The two sublattices (A or B) are indicated by color (red or blue). (b) Electron dispersion in a uniform AF state. Each subband is spin degenerate.

With a unitary transformation, $c_i = U_i\tilde{c}_i$, which diagonalizes the s-d coupling, $U_i^\dagger(\boldsymbol{n}_i\cdot\boldsymbol{\sigma})U_i = \sigma^z$, H is transformed into $H = -t\sum_{(i,j)}\tilde{c}_i^\dagger \mathrm{e}^{iA_{ij}}\tilde{c}_j - J\sum_i(-)^i\tilde{c}_i^\dagger\sigma^z\tilde{c}_i + u_\mathrm{i}\sum_i{}'\tilde{c}_i^\dagger\tilde{c}_i$, where $J = J_\mathrm{sd}S$, and A_{ij} is the spin gauge field defined by $U_i^\dagger U_j = \mathrm{e}^{iA_{ij}}$ [34,35]. Because of slow variations of the texture, A_{ij} is small and can be treated perturbatively. The unperturbed state (with $A_{ij} = 0$) is a uniform AF, and the electron band splits into spin-degenerate upper and lower bands, $\pm E_{\boldsymbol{k}}$, with an AF gap $2|J|$ in between [Fig. 1(b)]. Here, $E_{\boldsymbol{k}} \equiv \sqrt{\varepsilon_{\boldsymbol{k}}^2 + J^2}$ with $\varepsilon_{\boldsymbol{k}} = -2t(\cos k_x + \cos k_y)$. Also, A_{ij} can be treated in the continuum approximation, $A_{ij} \to A_\mu$, where μ $(= x, y)$ specifies the bond direction of (i, j), and expanded as

$$A_\mu = \tfrac{1}{2}A_\mu^\alpha\sigma^\alpha = \tfrac{1}{2}\left(A_\mu^z\sigma^z + \boldsymbol{A}_\mu^\perp\cdot\boldsymbol{\sigma}^\perp\right), \tag{5}$$

where $\alpha = x, y, z$ and $\perp = x, y$. The spin-conserving component A^z describes adiabatic processes, whereas the spin-flip component $\boldsymbol{A}^\perp$ induces nonadiabatic transitions. In FM, the latter can be important only in the weak-coupling regime [36], but in AF both are important because of spin degeneracy of the AF bands. Both produce the same effective field, $(\nabla\times\boldsymbol{A}^z)_z = (\boldsymbol{A}_x^\perp\times\boldsymbol{A}_y^\perp)^z = \boldsymbol{n}\cdot(\partial_x\boldsymbol{n}\times\partial_y\boldsymbol{n})$.

To calculate the spin Hall conductivity, $\sigma_\mathrm{SH} \equiv \frac{1}{2}(\sigma_{xy}^z - \sigma_{yx}^z)$, we assume a good AF metal and focus on the Fermi-surface contribution [37],

$$\sigma_{ij}^z(\boldsymbol{Q}) = -\frac{e\hbar}{4\pi}\mathrm{Tr}\left\langle\mathcal{J}_{\mathrm{s},i}^z G^\mathrm{R}_{\boldsymbol{k}_+,\boldsymbol{k}'}\mathcal{J}_j G^\mathrm{A}_{\boldsymbol{k}',\boldsymbol{k}_-}\right\rangle_\mathrm{i}, \tag{6}$$

where $\mathcal{J}_{\mathrm{s},i}^z$ and $\mathcal{J}_j$ are spin-current and number-current vertices, Tr means the trace in spin, sublattice, and $\boldsymbol{k}$ spaces ($\boldsymbol{k}$, $\boldsymbol{k}'$ integrals), and $\langle\cdots\rangle_\mathrm{i}$ represents impurity average. The Green's function $G^{\mathrm{R(A)}}_{\boldsymbol{k},\boldsymbol{k}'} = (\mu - H \pm i0)^{-1}_{\boldsymbol{k},\boldsymbol{k}'}$ takes full account of impurities and the gauge field, and $\boldsymbol{k}_\pm = \boldsymbol{k} \pm \boldsymbol{Q}/2$. We treat the impurity scattering in the Born approximation with ladder vertex corrections (VC) [38]. The superscript z on σ_{ij}^z and $\mathcal{J}_{\mathrm{s},i}^z$ indicates the spin component in the rotated frame, thus it is the component *projected to the local Néel vector* $\boldsymbol{n}$.

After a standard procedure (see the Supplemental Material [38]), we obtain Eq. (1) with $\tilde{\sigma}_\mathrm{SH} = \tilde{\sigma}_\mathrm{SH}^{(0)} + \tilde{\sigma}_\mathrm{SH}^{(1)}$,

$$\tilde{\sigma}_\mathrm{SH}^{(0)} = (J\tau)^2\frac{t^2\nu}{\mu}\left(1 - \frac{J^2}{\mu^2}\right)C_{xy}, \tag{7}$$

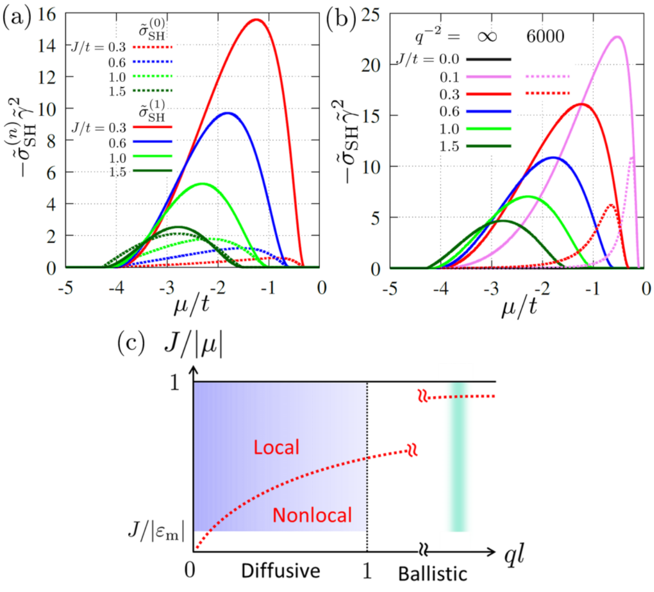

FIG. 2. (a), (b) Normalized topological spin Hall conductivity vs chemical potential μ for several choices of J/t. (a) $\tilde{\sigma}_\mathrm{SH}^{(0)}\tilde{\gamma}^2$ and $\tilde{\sigma}_\mathrm{SH}^{(1)}\tilde{\gamma}^2$, where $\tilde{\gamma} = \pi n_\mathrm{i}u_\mathrm{i}^2/t^2$ is a dimensionless damping parameter. (b) $\tilde{\sigma}_\mathrm{SH} = \tilde{\sigma}_\mathrm{SH}^{(0)} + \tilde{\sigma}_\mathrm{SH}^{(1)}$. In (b), $\tilde{\sigma}_\mathrm{SH}$ with finite q are also shown (dotted lines). These are odd functions of μ, hence plotted only for the lower AF band. The parameters used are $\tilde{\gamma} = 0.2$ and $\tau_\mathrm{s}^{-1} = 10^{-4}t$. (c) Characteristic parameter regions for the TSH conductivity. The red dashed line, given by $J/|\mu| = ql/\sqrt{4 + (ql)^2}$ in the diffusive regime, is a crossover line separating the local and nonlocal field regions, and $\varepsilon_\mathrm{m} = \sqrt{(4t)^2 + J^2}$. The analytical results, Eqs. (7), (8), and (13), apply to the blue shaded region, while the numerical results (Fig. 4) apply to the green shaded region.

$$\tilde{\sigma}_\mathrm{SH}^{(1)} = (J\tau)^2\frac{t^2\nu}{\mu}\frac{8t^2}{\mu^2 + J^2}\left(\frac{\tau^{-1}}{\tau_\varphi^{-1} + \tau_\mathrm{s}^{-1}}\right)C_{xx}^2, \tag{8}$$

where $\tilde{\sigma}_\mathrm{SH}^{(0)}$ is the contribution without VC, which comes from both adiabatic and nonadiabatic processes, and $\tilde{\sigma}_\mathrm{SH}^{(1)}$ is the contribution with VC, coming only from nonadiabatic processes. Here, $\nu = \nu(\mu)$ is the density of states (per spin) at chemical potential μ, $C_{ij} = \langle 1 - \cos k_i \cos k_j\rangle_\mathrm{FS}$ is the Fermi surface average [39], $\tau = [\gamma_0 + (J/\mu)\gamma_3]^{-1}/2$ is the scattering time [$\gamma_0 = \pi n_\mathrm{i}u_\mathrm{i}^2\nu$ and $\gamma_3 = (J/\mu)\gamma_0$ are the sublattice independent and dependent parts, respectively, of the damping, and n_i is the impurity concentration], and

$$\frac{1}{\tau_\varphi} = \frac{4J}{\mu}\frac{\mu^2 + J^2}{\mu^2 - J^2}\gamma_3 = \frac{2J^2}{\mu^2 - J^2}\frac{1}{\tau} \tag{9}$$

is the "spin dephasing" rate [40]. We introduced a finite spin relaxation rate τ_s^{-1} by hand [41]; without τ_s^{-1}, we would have an unphysical result that $\tilde{\sigma}_\mathrm{SH}^{(1)}$ does not vanish in the limit $J \to 0$. Note that τ_φ^{-1} differs from τ_s^{-1} in that it does not require spin-dependent scattering, randomizes only the transverse ($\perp \boldsymbol{n}$) components of the electron spin (see below), and vanishes as $J \to 0$. The results (7) and (8) are obtained at the leading order, i.e., second order in spatial gradient and second order in τ.

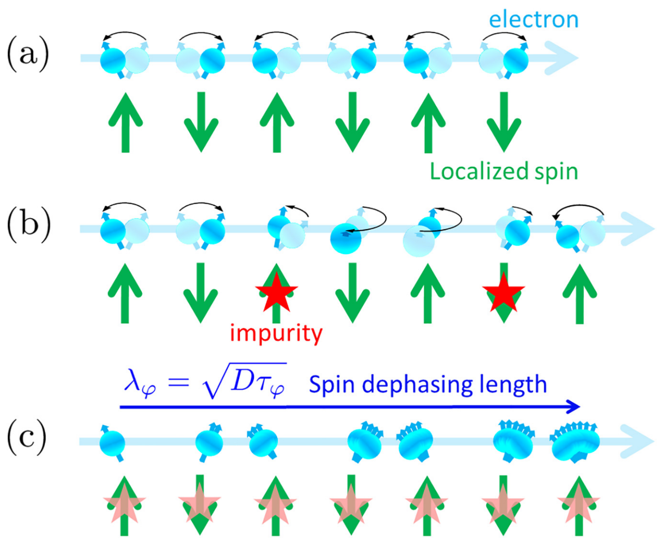

FIG. 3. Physical picture of electron spin transport in a uniform antiferromagnet. The blue sphere with an arrow represents an electron, the green arrow a localized spin, and the red star a nonmagnetic impurity. (a) The electron spin precesses around the local moment, alternating its sense from site to site. (b) Interaction with impurities locally modifies the precession. (c) A "collective" transverse spin density contributed from many electrons decays and loses its original information through the impurity scattering. This is because the degree of the modification, mentioned in (b), varies from electron to electron. This is called "dephasing" and the characteristic length is the "dephasing length" $\lambda_\varphi = \sqrt{D\tau_\varphi}$. The orange stars represent averaged impurities.

The coefficients $\tilde{\sigma}_{\mathrm{SH}}^{(0)}$ and $\tilde{\sigma}_{\mathrm{SH}}^{(1)}$ are plotted in Fig. 2(a). They are comparable in magnitude at large J ($\sim 1.5t$), but as J is reduced, $\tilde{\sigma}_{\mathrm{SH}}^{(1)}$ grows markedly, whereas $\tilde{\sigma}_{\mathrm{SH}}^{(0)}$ decreases. The sum $\tilde{\sigma}_{\mathrm{SH}} = \tilde{\sigma}_{\mathrm{SH}}^{(0)} + \tilde{\sigma}_{\mathrm{SH}}^{(1)}$ is plotted in Fig. 2(b) by solid lines, which grows as J is reduced, especially near the AF gap edge, but finally vanishes at $J = 0$. Since $\tilde{\sigma}_{\mathrm{SH}}^{(1)}$ comes solely from nonadiabatic processes, these results show that the combined effect of nonadiabaticity and the VC is important for the present SHE [42]. Physically, a nonadiabatic process produces a transverse spin polarization, and the VC describes its collective transport, which is however limited by spin dephasing [35,40,43]. The origin of the enhancement at small J can be traced to the reduced dephasing at small J [38]. As seen from Eq. (9), the spin dephasing arises through γ_3, a sublattice asymmetry in (nonmagnetic) scattering [35,44], and its physical picture is illustrated in Fig. 3.

The obtained result, Eq. (1), needs to be interpreted with care. It arises with the scalar chirality formed by the Néel vector $\boldsymbol{n}$, and changes sign under $\boldsymbol{n} \to -\boldsymbol{n}$. This is not a pleasant situation since any physical quantity measurable by (semi)macroscopic means should not depend on the sign of $\boldsymbol{n}$. This (apparent) puzzle is resolved if we note that the spin component of the calculated spin current $\tilde{j}^{\tilde{z}}_{x,\mathrm{s}}$ is the one projected to the Néel vector $\boldsymbol{n}$. Therefore, we write $\tilde{j}^{\tilde{z}}_{\mathrm{s}} = \boldsymbol{n}\cdot\boldsymbol{j}_{\mathrm{s}}$ and identify $\boldsymbol{j}_{\mathrm{s}}$ as a physical spin current. The physical spin Hall current is thus given by Eq. (2).

It is in fact possible to obtain Eq. (2) directly. By assuming J is small and treating it perturbatively, we found that a spin current arises at second order in J [38],

$$j^{\alpha}_{\mathrm{s},i} = (J\tau)^2 \frac{t^2\nu}{\mu} C_{xy} (\partial_i \boldsymbol{n} \times \partial_j \boldsymbol{n})^{\alpha} eE_j. \tag{10}$$

This contrasts with the THE in FM caused by scalar spin chirality, which starts at third order ($\sim J^3$) [10], and demonstrates that the essential quantity for the present SHE is the vector (not scalar) chirality. That Eq. (10) is an even function of J (or $J\boldsymbol{n}$) is consistent with the fact that the spin current is even under time reversal.

The expression Eq. (2) holds locally in space (as far as the variation of $\boldsymbol{n}$ is sufficiently slow). As a spin current measured experimentally, we consider a spatially averaged one, $\langle \boldsymbol{j}^{\alpha}_{\mathrm{s}} \rangle = \Omega^{-1} \int \boldsymbol{j}^{\alpha}_{\mathrm{s}} dxdy$ (in two dimensions), where Ω is the sample area. It can be written as

$$\langle \boldsymbol{j}^{\alpha}_{\mathrm{s}} \rangle = \pi \tilde{\sigma}_{\mathrm{SH}} \frac{m^{\alpha}}{\Omega} (e\boldsymbol{E} \times \hat{z}), \tag{11}$$

where

$$m^{\alpha} = \frac{1}{2\pi} \int (\nabla \times \boldsymbol{a}^{\alpha})_z dxdy = \frac{1}{2\pi} \oint \boldsymbol{a}^{\alpha} \cdot d\boldsymbol{\ell}, \tag{12}$$

and $a^{\alpha}_i = (\boldsymbol{n} \times \partial_i \boldsymbol{n})^{\alpha}$ [Eq. (3)] is an emergent vector potential in spin channel. The line integral is taken along the sample perimeter. If the system has easy-plane magnetic anisotropy, and the Néel vector on the sample edge is constrained to lie in plane, e.g., x-y plane, the line integral of the vector chirality defines a topological winding number $m^z \in \mathbb{Z}$ in $\pi_1(S^1)$. The spin Hall conductivity is thus proportional to the topological number density m^z/Ω, and this fact resurrects the naming "topological" spin Hall effect. We emphasize that it is characterized by the vector chirality of the Néel vector along the sample edge. Therefore, the present TSHE is absent for AF skyrmions, in which the Néel vector at the edge is uniaxial. On the other hand, it is finite for AF merons, which have finite in-plane winding of the Néel vector along the edge.

To verify these results, we have conducted numerical works based on the four-terminal Landauer-Büttiker formula [38,45,46]. We consider ballistic systems with $L \times L$ sites without disorder, and containing a single AF skyrmion or a single AF meron. For both textures, the spin Hall conductance G^{z}_{SHC} shows a strong peak just below the AF gap [Figs. 4(a) and 4(b)], which, however, behave oppositely as L is increased (with the skyrmion/meron size fixed); for the AF skyrmion the peak decreases with L and seems to vanish in the thermodynamic limit. In contrast, for the AF meron it increases with L [Fig. 4(c)]. This is consistent with the analytical result, which is valid for infinite-size systems. Plots for several J/t values are shown in Fig. 4(d) for the AF meron system, showing that it is indeed enhanced at small J/t. All these features agree with the analytic results, except for the detailed shape of μ dependence.

The discrepancy in shape (μ dependence) between the numerical [Fig. 4(d)] and analytic results [Fig. 2(b)] may be understood as due to the nonlocality effect in the former. To illustrate this, let us first consider the diffusive regime. As the typical wave number q of the Néel texture (i.e., inverse of meron/skyrmion size) is increased, Eq. (8) is modified as

$$\left(\tau_{\varphi}^{-1} + \tau_{\mathrm{s}}^{-1}\right)^{-1} \to \left(\tau_{\varphi}^{-1} + \tau_{\mathrm{s}}^{-1} + Dq^2\right)^{-1} \tag{13}$$

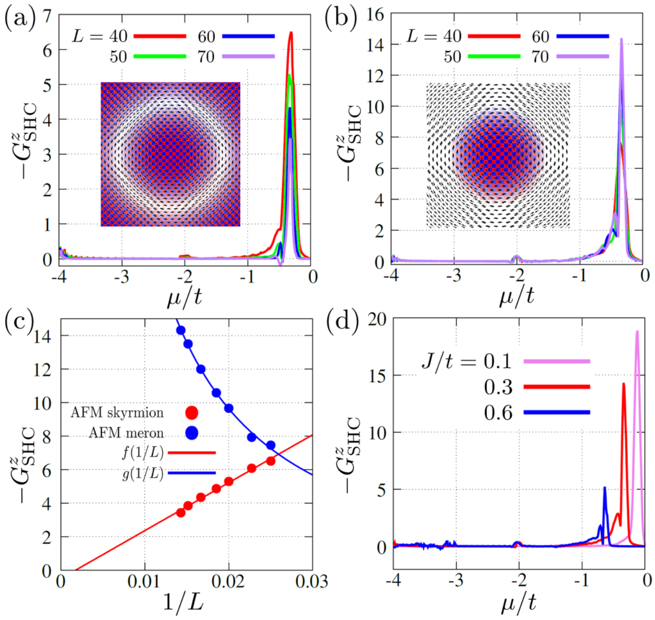

FIG. 4. Topological spin Hall conductance ($G^z_{\rm SHC}$) based on the Landauer-Büttiker formula for finite systems with $L \times L$ sites. (a) AF skyrmion system. (b) AF meron system. (c) L dependence of the peak value of $G^z_{\rm SHC}$. The data are fitted with functions, $f(x) = 286x - 0.504$ and $g(x) = 0.237/x - 2.22$. (d) AF meron system with $L = 70$ for several choices of J/t. We took $J/t = 0.3$ [except in (d)] and meron/skyrmion radius $r = 15$. The data are symmetrized with respect to $J \to -J$, as explained in [38].

in the denominator, where D is the diffusion constant. When electron spin diffusion (Dq^2) occurs faster than spin dephasing (τ_φ^{-1}), the effective field becomes "nonlocal." A similar feature has been noted for FMs, in which Dq^2 is compared to the exchange splitting [36]. Here in AF, it is compared to the (much smaller) spin dephasing rate, τ_φ^{-1}, hence the present SHE enters the nonlocal regime rather easily compared to the THE in FM. More explicitly, the nonlocality appears if

$$ql > \frac{2J}{\sqrt{\mu^2 - J^2}}, \quad \text{or} \quad |\mu| > J\sqrt{1 + (2/ql)^2}, \tag{14}$$

where l is the mean free path. In Fig. 2(b), the analytic results with $q^{-2} = 6000$ (with lattice constant taken unity) are plotted by dotted lines. The suppression due to nonlocality is more significant at larger $|\mu|$ (away from the AF gap), leaving a sharp peak in the vicinity of the AF gap edge. Since cleaner systems enter the nonlocal regime more easily [see Eq. (14) and a red dotted line in Fig. 2(c)], this feature is expected to persist into the ballistic regime with a wider nonlocality region. The shape of Fig. 4(d) may thus be understood as due to the nonlocality effect.

Thus, as in the case of THE in FM [36], the present TSHE in AF exhibits various characteristic regimes [Fig. 2(c)]. These are summarized as follows. First, for a ballistic and local regime, the effect is truly topological. As q is increased and the nonlocal effects become important, the SHC deviates from the topological expression. In the diffusive case, it is difficult to have the topological expression because of dephasing (and nonlocality), but the effect is enhanced for weak-coupling AF with a small AF gap. An interesting possibility may be found in mesoscopic systems, for which the effect can be topological even if the system is in a diffusive regime.

The emergent vector potential $\boldsymbol{a}^\alpha$ in the spin channel, identified here through TSHE, has more generality. In a study on THE in canted AF [35], an emergent vector potential in the charge channel was identified as $l^\alpha \boldsymbol{a}^\alpha$, where l^α is the canting (uniform) moment. Also, $\boldsymbol{a}^\alpha$ can be expressed as $a_i^\alpha = -(\mathcal{R}\boldsymbol{A}_i^\perp)^\alpha$ [47], where $\mathcal{R}$ is an SO(3) matrix that connects the rotated and the original frames (e.g., $\boldsymbol{n} = \mathcal{R}\hat{z}$), showing its conformity with the spin gauge field $\boldsymbol{A}_i^\perp$. These facts reinforce our interpretation of $\boldsymbol{a}^\alpha$ as an effective vector potential in the spin channel.

To realize the present TSHE experimentally, a prime candidate texture is $\boldsymbol{n}$ meron. Such a texture was found very recently in insulating α-Fe$_2$O$_3$ [24], and also in semimetallic CuMnAs [25]. Another candidate is a canted AF; if the ferromagnetic moment $\boldsymbol{l}$ (due to canting) forms a skyrmion (called "$\boldsymbol{l}$ skyrmion" in [35]), topological consideration shows that the Néel vector winds at least twice around the skyrmion, i.e., $m^z = 2$ per skyrmion [35,48]. A recent experiment on thin films of Ce-doped CaMnO$_3$, a canted AF, observed skyrmion bubbles formed by the (weak) ferromagnetic moment [49]. Therefore, this system can also be a candidate for the present TSHE. Moreover, a method to detect the chirality of AF texture has been proposed [26], which will promote the study of AF texture-induced phenomena. Finally, we note that a meron-antimeron lattice with different core sizes [50] offers a good candidate that integrates the present effect; if the nonlocality effect suppresses the topological contribution of the smaller one (e.g., antimeron), the complete cancellation between meron and antimeron can be avoided.

Several theoretical works have been reported on the TSHE in AF based on scalar chirality [15–17]. In Ref. [16], the authors considered AF skyrmion lattices, and calculated intrinsic (Berry curvature) contributions projected on local spins $\boldsymbol{s}_i \sim (-)^i\boldsymbol{n}$. Experimentally, in a closely related phenomenon, i.e., THE in a FM skyrmion lattice, the measured conductivity data scale like $\sim\tau^2$ [51,52], indicating a primary importance of the Fermi-surface contribution as we have calculated in this Letter. In Ref. [17], the authors used the Landauer-Büttiker method to find a nonzero TSHE in systems with an AF skyrmion, and examined a torque acting on the skyrmion. Their result does not contradict with our result because of finite system size, but our result suggests that it vanishes in the thermodynamic limit. They expressed the induced spin current as $j^\alpha_{{\rm s},i} \sim n^\alpha\,[\boldsymbol{n}\cdot(\partial_i\boldsymbol{n} \times \partial_j\boldsymbol{n})]E_j$, which is essentially the same as Eq. (2) (and is convenient to obtain a torque), but it does not express a topological density because of the extra factor of n^α. (The topological aspect of the effect has been misidentified so far). They also pointed out an increase of the TSH conductivity for special impurity configurations. It would be interesting to study how the impurity configuration affects spin dephasing and the TSHE.

The emergence of vector chirality is not a surprise. Rather, it has good chemistry with spin currents, just as the good chemistry of scalar chirality with charge currents [7–11]. The present work extends this picture to nonequilibrium spin currents beyond equilibrium ones [21–23]. The appearance of the TSHE at second (not third) order in J disproves any scenario based on scalar chirality.

To summarize, we have studied a spin Hall effect due to magnetic textures in AF metals. By analytic calculations, we found a topological contribution proportional to the winding number defined by vector chirality, suggesting that the TSHE in AF is characterized by a homotopy class $\pi_1(S^1)$, different from $\pi_2(S^2)$ of the THE in ferromagnets. This is finite for AF merons but not for AF skyrmions, and is enhanced at weak coupling. These results are confirmed by numerical calculations based on the Landauer-Büttiker formula. Important roles played by nonadiabatic processes and spin dephasing are pointed out. The results obtained in this work will provide hints to experiments exploring enhanced spin currents and texture-based functionalities in antiferromagnets.

We would like to thank J. Fujimoto, Y. Imai, A. Matsui, M. Mostovoy, T. Nomoto, R. Yambe, T. Yamaguchi, and A. Yamakage for valuable discussions. This work was partly supported by JSPS KAKENHI Grants No. JP15H05702, No. JP17H02929, No. JP19K03744, and No. JP21H01799, and the Center of Spintronics Research Network of Japan. K.N. is supported by JSTCREST (JP-MJCR18T2) and JSPS KAKENHI Grant No. JP21K13875. J.J.N. is supported by a Program for Leading Graduate Schools "Integrative Graduate Education and Researchin Green Natural Sciences" and Grant-in-Aid for JSPS Research Fellow Grant No. JP19J23587.

---

[1] J. Sinova, S. O. Valenzuela, J. Wunderlich, C. H. Back, and T. Jungwirth, Spin Hall effects, Rev. Mod. Phys. **87**, 1213 (2015).

[2] M. I. Dyakonov and V. I. Perel, Possibility of orienting electron spins with current, JETP Lett. **13**, 467 (1971); Current-induced spin orientation of electrons in semiconductors, Phys. Lett. A **35**, 459 (1971).

[3] S. Murakami, N. Nagaosa, and S.-C. Zhang, Dissipationless quantum spin current at room temperature, Science **301**, 1348 (2003).

[4] J. Sinova, D. Culcer, Q. Niu, N. A. Sinitsyn, T. Jungwirth, and A. H. MacDonald, Universal intrinsic spin Hall effect, Phys. Rev. Lett. **92**, 126603 (2004).

[5] Y. K. Kato, R. C. Myers, A. C. Gossard, and D. D. Awschalom, Observation of the spin Hall effect in semiconductors, Science **306**, 1910 (2004).

[6] J. Wunderlich, B. Kaestner, J. Sinova, and T. Jungwirth, Experimental observation of the spin-Hall effect in a two-dimensional spin-orbit coupled semiconductor system, Phys. Rev. Lett. **94**, 047204 (2005).

[7] D. Loss and P. Goldbart, Period and amplitude halving in mesoscopic rings with spin, Phys. Rev. B **43**, 13762 (1991).

[8] J. Ye, Y. B. Kim, A. J. Millis, B. I. Shraiman, P. Majumdar, and Z. Tesanovic, Berry phase theory of the anomalous Hall effect: Application to colossal magnetoresistance manganites, Phys. Rev. Lett. **83**, 3737 (1999).

[9] K. Ohgushi, S. Murakami, and N. Nagaosa, Spin anisotropy and quantum Hall effect in the kagomé lattice: Chiral spin state based on a ferromagnet, Phys. Rev. B **62**, R6065(R) (2000).

[10] G. Tatara and H. Kawamura, Chirality-driven anomalous Hall effect in weak coupling regime, J. Phys. Soc. Jpn. **71**, 2613 (2002).

[11] P. Bruno, V. K. Dugaev, and M. Taillefumier, Topological Hall effect and Berry phase in magnetic nanostructures, Phys. Rev. Lett. **93**, 096806 (2004).

[12] This applies to the strong s-d coupling regime. In the weak-coupling regime, there is a proposal recently that the essence is the Hall effect in the charge channel [13].

[13] K. S. Denisov, I. V. Rozhansky, N. S. Averkiev, and E. Lähderanta, Electron scattering on a magnetic Skyrmion in the nonadiabatic approximation, Phys. Rev. Lett. **117**, 027202 (2016); General theory of the topological Hall effect in systems with chiral spin textures, Phys. Rev. B **98**, 195439 (2018); I. V. Rozhansky, K. S. Denisov, M. B. Lifshits, N. S. Averkiev, and E. Lähderanta, Topological and chiral spin Hall effects, Phys. Status Solidi (b) **256**, 1900033 (2019).

[14] J. B. S. Mendes, R. O. Cunha, O. Alves Santos, P. R. T. Ribeiro, F. L. A. Machado, R. L. Rodríguez-Suárez, A. Azevedo, and S. M. Rezende, Large inverse spin Hall effect in the antiferromagnetic metal $Ir_{20}Mn_{80}$, Phys. Rev. B **89**, 140406(R) (2014).

[15] P. M. Buhl, F. Freimuth, S. Blügel, and Y. Mokrousov, Topological spin Hall effect in antiferromagnetic skyrmions, Phys. Status Solidi RRL **11**, 1700007 (2017).

[16] B. Göbel, A. Mook, J. Henk, I. Mertig, Antiferromagnetic skyrmion crystals: Generation, topological Hall, and topological spin Hall effect, Phys. Rev. B **96**, 060406(R) (2017).

[17] C. A. Akosa, O. A. Tretiakov, G. Tatara, and A. Manchon, Theory of the topological spin Hall effect in antiferromagnetic skyrmions: Impact on current-induced motion, Phys. Rev. Lett. **121**, 097204 (2018).

[18] One may also think of Néel vector chirality, which, however, has more flavor of scalar chirality formed by the Néel vector, i.e., $\boldsymbol{n} \cdot (\partial_i \boldsymbol{n} \times \partial_j \boldsymbol{n})$.

[19] K. Taguchi and G. Tatara, Anomalous Hall conductivity due to vector spin chirality in the weak coupling regime, Phys. Rev. B **79**, 054423 (2009).

[20] H. Ishizuka and N. Nagaosa, Impurity-induced vector spin chirality and anomalous Hall effect in ferromagnetic metals, New J. Phys. **20**, 123027 (2018).

[21] G. Tatara and N. Garcia, Quantum toys for quantum computing: Persistent currents controlled by the spin Josephson effect, Phys. Rev. Lett. **91**, 076806 (2003).

[22] H. Katsura, N. Nagaosa, and A. V. Balatsky, Spin current and magnetoelectric effect in noncollinear magnets, Phys. Rev. Lett. **95**, 057205 (2005).

[23] T. Kikuchi, T. Koretsune, R. Arita, and G. Tatara, Dzyaloshinskii-Moriya interaction as a consequence of a doppler shift due to spin-orbit-induced intrinsic spin current, Phys. Rev. Lett. **116**, 247201 (2016).

[24] H. Jani, J.-C. Lin, J. Chen, J. Harrison, F. Maccherozzi, J. Schad, S. Prakash, C.-B. Eom, A. Ariando, T. Venkatesan, and

P. G. Radaelli, Antiferromagnetic half-skyrmions and bimerons at room temperature, Nature (London) **590**, 74 (2021).

[25] O. J. Amin, S. F. Poole, S. Reimers, L. X. Barton, A. Dal Din, F. Maccherozzi, S. S. Dhesi, V. Novák, F. Krizek, J. S. Chauhan, R. P. Campion, A. W. Rushforth, T. Jungwirth, O. A. Tretiakov, K. W. Edmonds, and P. Wadley, Antiferromagnetic half-skyrmions electrically generated and controlled at room temperature, Nat. Nanotechnol. **18**, 849-853 (2023).

[26] A. K. C. Tan, H. Jani, M. Högen, L. Stefan, C. Castelnovo, D. Braund, A. Geim, A. Mechnich, M. S. G. Feuer, H. S. Knowles, A. Ariando, P. G. Radaelli, and M. Atatüre, Revealing emergent magnetic charge in an antiferromagnet with diamond quantum magnetometry, Nat. Mater. **23**, 205-211 (2024).

[27] C. Jin, C. Song, J. Wang, and Q. Liu, Dynamics of antiferromagnetic skyrmion driven by the spin Hall effect, Appl. Phys. Lett. **109**, 182404 (2016).

[28] X. Zhang, Y. Zhou, and M. Ezawa, Antiferromagnetic skyrmion: Stability, creation and manipulation, Sci. Rep. **6**, 24795 (2016).

[29] H. Velkov, O. Gomonay, M. Beens, G. Schwiete, A. Brataas, J. Sinova, and R. A. Duine, Phenomenology of current-induced skyrmion motion in antiferromagnets, New J. Phys. **18**, 075016 (2016).

[30] J. Barker and O. A. Tretiakov, Static and dynamical properties of antiferromagnetic skyrmions in the presence of applied current and temperature, Phys. Rev. Lett. **116**, 147203 (2016).

[31] T. Dohi, S. DuttaGupta, S. Fukami, and H. Ohno, Formation and current-induced motion of synthetic antiferromagnetic skyrmion bubbles, Nat. Commun. **10**, 5153 (2019).

[32] W. Legrand, D. Maccariello, F. Ajejas, S. Collin, A. Vecchiola, K. Bouzehouane, N. Reyren, V. Cros, and A. Fert, Room-temperature stabilization of antiferromagnetic skyrmions in synthetic antiferromagnets, Nat. Mater. **19**, 34 (2020).

[33] R. Yambe and S. Hayami, Ferrochiral, antiferrochiral, and ferrichiral skyrmion crystals in an itinerant honeycomb magnet, Phys. Rev. B **107**, 014417 (2023).

[34] G. Tatara, H. Kohno, and J. Shibata, Microscopic approach to current-driven domain wall dynamics, Phys. Rep. **468**, 213 (2008).

[35] J. J. Nakane, K. Nakazawa, and H. Kohno, Topological Hall effect in weakly canted antiferromagnets, Phys. Rev. B **101**, 174432 (2020).

[36] K. Nakazawa, M. Bibes, and H. Kohno, Topological Hall effect from strong to weak coupling, J. Phys. Soc. Jpn. **87**, 033705 (2018); K. Nakazawa, and H. Kohno, Weak coupling theory of topological Hall effect, Phys. Rev. B **99**, 174425 (2019).

[37] P. Středa, Theory of quantised Hall conductivity in two dimensions, J. Phys. C **15**, L717 (1982).

[38] See Supplemental Material at http://link.aps.org/supplemental/10.1103/PhysRevB.109.L241105 for calculation details, explicit formulas of the adiabatic and nonadiabatic contributions, analysis on the enhancement at weak coupling, perturbative treatment of J, and further plots including the spin Hall angle.

[39] Explicitly, they are evaluated as [35]

$$C_{xy} = \frac{1}{4\pi^2}\frac{|\mu|}{t^2 v}\left[\frac{2}{\tilde{\mu}}K(x) - \left(1+\frac{1}{\tilde{\mu}}\right)E(x)\right],$$

$$C_{xx} = \frac{1}{4\pi^2}\frac{|\mu|}{t^2 v}\left[\left(1+\frac{1}{\tilde{\mu}}\right)E(x) - 2K(x)\right],$$

where $K(x)$ and $E(x)$ are the complete elliptic integrals of the first and the second kind, respectively, and $\tilde{\mu} = \sqrt{\mu^2 - J^2}/4t$ and $x = (1-\tilde{\mu})/(1+\tilde{\mu})$ are dimensionless parameters.

[40] A. Manchon, Spin diffusion and torques in disordered antiferromagnets, J. Phys.: Condens. Matter **29**, 104002 (2017). Their β seems to be $\sin \chi_{k_\mathrm{F}}$ instead of $\cos \chi_{k_\mathrm{F}}$.

[41] A microscopic calculation of the spin relaxation rate in AF metal can be found in Ref. [44], in which magnetic impurities are considered as a spin sink.

[42] The nonadiabatic process is important at a more fundamental level. Both the adiabatic and nonadiabatic contributions to $\tilde{\sigma}_{\mathrm{SH}}^{(0)}$ contain terms of $O(J^0)$, which do not vanish at $J = 0$, but when added they cancel each other and the resulting $\tilde{\sigma}_{\mathrm{SH}}^{(0)}$ vanishes at $J = 0$ [38].

[43] S. Hikami, A. I. Larkin, and Y. Nagaoka, Spin-orbit interaction and magnetoresistance in the two dimensional random system, Prog. Theor. Phys. **63**, 707 (1980).

[44] J. J. Nakane and H. Kohno, Microscopic calculation of spin torques in textured antiferromagnets, Phys. Rev. B **103**, L180405 (2021).

[45] J. Ohe, T. Ohtsuki, and B. Kramer, Mesoscopic Hall effect driven by chiral spin order, Phys. Rev. B **75**, 245313 (2007).

[46] N. Romming, A. Kubetzka, C. Hanneken, K. von Bergmann, and R. Wiesendanger, Field-dependent size and shape of single magnetic skyrmions, Phys. Rev. Lett. **114**, 177203 (2015).

[47] H. Kohno and J. Shibata, Gauge field formulation of adiabatic spin torques, J. Phys. Soc. Jpn. **76**, 063710 (2007).

[48] O. Meshcheriakova, S. Chadov, A. K. Nayak, U. K. Rößler, J. Kübler, G. André, A. A. Tsirlin, J. Kiss, S. Hausdorf, A. Kalache, W. Schnelle, M. Nicklas, and C. Felser, Large noncollinearity and spin reorientation in the novel $\mathrm{Mn_2RhSn}$ Heusler magnet, Phys. Rev. Lett. **113**, 087203 (2014).

[49] L. Vistoli, W. Wang, A. Sander, Q. Zhu, B. Casals, R. Cichelero, A. Barthélémy, S. Fusil, G. Herranz, S. Valencia, R. Abrudan, E. Weschke, K. Nakazawa, H. Kohno, J. Santamaria, W. Wu, V. Garcia, and M. Bibes, Giant topological Hall effect in correlated oxide thin films, Nat. Phys. **15**, 67 (2019).

[50] A ferromagnetic counterpart has been reported in: S.-Z. Lin, A. Saxena, and C. D. Batista, Skyrmion fractionalization and merons in chiral magnets with easy-plane anisotropy, Phys. Rev. B **91**, 224407 (2015).

[51] N. Kanazawa, Y. Onose, T. Arima, D. Okuyama, K. Ohoyama, S. Wakimoto, K. Kakurai, S. Ishiwata, and Y. Tokura, Large topological Hall effect in a short-period helimagnet MnGe, Phys. Rev. Lett. **106**, 156603 (2011).

[52] C. Franz, F. Freimuth, A. Bauer, R. Ritz, C. Schnarr, C. Duvinage, T. Adams, S. Blügel, A. Rosch, Y. Mokrousov, and C. Pfleiderer, Real-space and reciprocal-space berry phases in the Hall effect of $\mathrm{Mn_{1-x}Fe_xSi}$, Phys. Rev. Lett. **112**, 186601 (2014).